The Astrophysical Journal, 798:21 (10pp), 2015 January 1 doi:10.1088/0004-637X/798/1/21

MONTE CARLO SIMULATION OF METASTABLE OXYGEN PHOTOCHEMISTRY IN COMETARY ATMOSPHERES

D. V. Bisikalo[1], V. I. Shematovich[1], J.-C. Gérard[2], E. Jehin[3], A. Decock[3], D. Hutsemékers[4], J. Manfroid[5], and B. Hubert[2]
[1] Institute of Astronomy of the Russian Academy of Sciences, Moscow, Russia
[2] Laboratory for Planetary and Atmospheric Physics (LPAP), University of Liège, Liège, Belgium; B.Hubert@ulg.ac.be
[3] Origines Cosmologiques et Astrophysiques (ORCA), University of Liège, Belgium
[4] Extragalactic Astrophysics and Space Observations (EASO), University of Liège, Belgium
[5] High Energy Astrophysics Group (GAPHE), University of Liège, Belgium
Received 2014 February 21; accepted 2014 October 19; published 2014 December 15

ABSTRACT

Cometary atmospheres are produced by the outgassing of material, mainly H_2O, CO, and CO_2 from the nucleus of the comet under the energy input from the Sun. Subsequent photochemical processes lead to the production of other species generally absent from the nucleus, such as OH. Although all comets are different, they all have a highly rarefied atmosphere, which is an ideal environment for nonthermal photochemical processes to take place and influence the detailed state of the atmosphere. We develop a Monte Carlo model of the coma photochemistry. We compute the energy distribution functions (EDF) of the metastable $O(^1D)$ and $O(^1S)$ species and obtain the red (630 nm) and green (557.7 nm) spectral line shapes of the full coma, consistent with the computed EDFs and the expansion velocity. We show that both species have a severely non-Maxwellian EDF, that results in broad spectral lines and the suprathermal broadening dominates due to the expansion motion. We apply our model to the atmosphere of comet C/1996 B2 (Hyakutake) and 103P/Hartley 2. The computed width of the green line, expressed in terms of speed, is lower than that of the red line. This result is comparable to previous theoretical analyses, but in disagreement with observations. We explain that the spectral line shape does not only depend on the exothermicity of the photochemical production mechanisms, but also on thermalization, due to elastic collisions, reducing the width of the emission line coming from the $O(^1D)$ level, which has a longer lifetime.

Key words: comets: general – methods: numerical – techniques: spectroscopic

1. INTRODUCTION

Comets are relatively small sized bodies formed at the early stages of the solar system evolution some 4.6 billion years ago. They are often considered potential tracers of conditions prevailing at that time (Ehrenfreund & Charnley 2000). They mainly consist of an icy water nucleus with other constituents such as carbon monoxide (CO), carbon dioxide (CO_2), and dust. When these bodies escape their reservoirs, mainly the Oort cloud and the Kuiper belt, and approach the sun, they slowly warm up under the effect of solar radiation and their ices start to sublimate, releasing water vapor, CO, CO_2, dust, and other minor species. This process produces a large, highly rarefied, expanding atmosphere: the coma, surrounding the icy nucleus.

The coma is exposed to the Sun radiation and, in particular, to the ultraviolet solar flux, which is capable of triggering photochemical processes such as dissociation and ionization of the gaseous material. The complex photochemistry of the coma constituents has been the subject of many theoretical and observational studies. For example, Bhardwaj & Raghuram (2012) developed a photochemical model of the coma of comet C/1996 B2 (Hyakutake) to analyze the metastable oxygen $O(^1D)$ and $O(^1S)$ populations and emissions accounting for photodissociation and electron impact dissociation of H_2O, OH, CO, and CO_2, as well as the dissociative recombination of ions H_2O^+, OH^+, CO^+, and CO_2^+, and direct electron impact on oxygen atoms. The loss mechanisms of metastable oxygen included radiative decay, quenching, and reactions with H_2O, CO and CO_2. The densities of the major species of the coma (H_2O, CO, CO_2, and OH) were given by a Haser model (Biver et al. 1999). Bhardwaj & Raghuram (2012) conducted an analysis aimed at matching the observed and computed ratio of the 557.7 nm green emission of $O(^1S)$ to the 630.0 and 636.4 nm red emissions of $O(^1D)$, from which they estimated the CO_2 abundance and several photochemical parameters. Raghuram & Bhardwaj (2012) also applied the same model with adapted parameters to comet C/1995 Hale Bopp.

The OI green and red cometary emissions have been observed for long (Swings 1962). The green line at 557.7339 nm is emitted by the transition $O(^1S) \rightarrow O(^1D)$, populating the upper level of the red doublet of lines at 630.0304 and 636.3776 nm, which result from the transition $O(^1D) \rightarrow O(^3P)$. Because both red lines share the same common upper state, their intensity is in the ratio of their Einstein transition parameters (∼3.1). $O(^1S)$ has a radiative life time of ∼0.8 s, while the $O(^1D) \rightarrow O(^3P)$ transition is strongly forbidden by Laporte's rule so that the ^1D state has an ∼110 s radiative lifetime. Festou & Feldman (1981) analyzed the production of metastable oxygen by photodissociation of CO_2 and H_2O and proposed that the different branching ratios of the $O(^1D)$ and $O(^1S)$ atoms from these parent molecules offer a mean to estimate the CO_2 abundance of the coma, relative to H_2O. Cochran (2008) observed the $O(^1S)$ and $O(^1D)$ emissions of the comae of six different comets and estimated their FWHM. In particular, they estimated that comet C/1996 B2 (Hyakutake), located at a heliocentric distance of 1.37 AU at the time of observation, presented velocity FWHM's of ∼1 km s^{-1} for the red line and 2.4 km s^{-1} for the green line, with an intensity ratio between the green line and the red doublet ranging between 1.3 and 1.6. Morrisson et al. (1997) observed comet C/1996 B2 (Hyakutake) at an ∼1 AU heliocentric distance and found the green/red ratio to be ∼1.3, but they could not resolve the shape of the spectral lines and determine their widths. Cochran

Table 1
Unattenuated Photoreaction Rates R (per parent molecule) and Average Exothermicity ΔE of the Processes Generating Metastable Oxygen Atoms, Under Minimum Solar Activity Conditions

		H_2O	CO	OH	CO_2
$O(^1D)$	R (s^{-1})	5.97×10^{-7}	3.47×10^{-8}	7.01×10^{-6}	9.24×10^{-7}
	ΔE (eV)	3.84	2.29	7.73	4.34
$O(^1S)$	R (s^{-1})	4.8×10^{-8}	3.95×10^{-8}	8.33×10^{-7}	4.40×10^{-7}
	ΔE (eV)	0.45	1.95	10	3.06

Notes. For $O(^1D)$, all numbers are derived from Huebner et al. (1992). For $O(^1S)$, only the numbers for OH are based on Huebner et al. (1992) while the other reaction rates are derived from the procedure described by Bhardwaj & Raghuram (2012).

(2008) concluded that the oxygen atoms in both metastable states were produced by the same parent molecules, after absorption of photons at different energies. Decock et al. (2013) analyzed the oxygen green and red emissions from 12 different comets detected from the ground with a high spectral resolution using the UVES spectrograph mounted on the 8 m Kueyen telescope of the ESO VLT (Dekker et al. 2000). They estimated the intensity ratio and the FWHM of both emissions. They concluded that H_2O is the main parent molecule of both states at low heliocentric distance, below ∼2 AU, while CO_2 was the most likely dominant parent molecule above ∼2.5 AU. They also found that the green line had a broader width than the red emissions, in contrast with theoretical estimates of Festou (1981).

Monte Carlo simulations were also conducted to simulate the gas flow in the Knudsen layer (Bisikalo et al. 1989), the coma photochemistry (Marov et al. 1996) and the coma dynamics (Tenishev et al. 2001, 2008; Rubin 2011; Combi 1996), applying the Direct Simulation Monte Carlo (DSMC) method (Bird 1994 and references therein). These simulations were mainly aimed at describing the complex interaction of the coma gas and dust that produce the acceleration of the material up to an expansion velocity of 0.8–1.2 km s^{-1}. It was shown that the asymptotic velocity is reached across distances on the order of a few nucleus radii, i.e., a few tens of kilometers to be compared with the several thousands of kilometers extension of the coma.

In this study, we develop a Monte Carlo model of the metastable $O(^1D)$ and $O(^1S)$ photochemistry to simulate the spectral line shape of the green and red emissions of oxygen. We compute the energy distribution functions of both species in the coma and use them to obtain the line-of-sight integrated emission of the full coma. We apply the model to the case of the comet C/1996 B2 (Hyakutake), at 1 AU under minimum solar activity conditions. We compare the spectral width of both emissions and compare our results with the observations of Decock et al. (2013) and Cochran (2008).

2. THE MONTE CARLO MODEL

We develop a Monte Carlo simulation model of the oxygen photochemistry in the cometary coma, assumed at steady state with a spherical geometry. This model produces a stochastic solution of the Boltzmann integro-differential equation with sources and sinks, and computes the energy distribution function of the $O(^1S)$ and $O(^1D)$ metastable species. We do not attempt to model the hydrodynamic expansion process: the coma is assumed to expand at a constant velocity, an approximation that is fully valid at cometocentric distances (r) above a few nucleus radii. We restrict the modeling domain to ∼5000 km of cometocentric distance (r) due to the heavy computational cost of such a computation. Up to these distances, Bhardwaj & Raghuram (2012) have shown that the most important sources of metastable oxygen are the photodissociation of H_2O, CO_2, CO, and OH (with, in addition, the 557.7 nm transition from $O(^1S)$, which produces $O(^1D)$). We thus neglect any electron-induced production mechanisms, such as the dissociative recombination of molecular ions and the electron-impact dissociation of molecules. Indeed, according to the modeling of comet C/1996 B2 (Hyakutake) by Bhardwaj & Raghuram (2012), photodissociation processes and radiation decay from $O(^1S)$ still contribute more than 80% of the total production rate of $O(^1D)$ at a cometocentric distance of ∼5000 km. Concerning the production of $O(^1S)$, our approximation is somewhat less accurate: at cometocentric distances below 1000 km, photodissociation processes contribute more than 80% of the total $O(^1S)$ production rate, but at 5000 km, this proportion falls to ∼65% so that extending our model beyond that cometocentric distance would be really unsafe. The reactions producing metastable oxygen that were accounted for in the model are listed in Equation (1):

$$\begin{cases} H_2O + h\upsilon \rightarrow \begin{cases} O(^1S) \\ O(^1D) \end{cases} + H_2 \\ CO_2 + h\upsilon \rightarrow \begin{cases} O(^1S) \\ O(^1D) \end{cases} + CO \\ CO + h\upsilon \rightarrow \begin{cases} O(^1S) \\ O(^1D) \end{cases} + C \\ OH + h\upsilon \rightarrow \begin{cases} O(^1S) \\ O(^1D) \end{cases} + H \\ O(^1S) \rightarrow O(^1D) + h\upsilon_{557.7}. \end{cases} \quad (1)$$

The loss mechanisms included in the model are the radiative decay and the collisional quenching of metastable atoms by collision with H_2O, CO_2, and CO. The production mechanisms listed in Equation (1) are exothermal, and the energy released in the process depends on that of the incident photon. We use the ultraviolet solar spectrum of Huebner et al. (1992) and their associated photochemical rates to compute the source rates and exothermicity of processes (1). The average reaction rates and exothermicities obtained under minimal solar activity are listed in Table 1. These numbers slightly differ from those of Bhardwaj & Raghuram (2012) because Huebner et al. (1992) used a different solar spectrum, and because we selected the experimental rate for OH rather than the theoretical value. The exothermicity is shared between the products with a weight that is inversely proportional to their mass (in a frame of reference moving with the center of mass of the dissociating products). The typical energy of an $O(^1D)$ atom produced by the photodissociation of H_2O is thus ∼0.43 eV. During their radiative lifetime (characterized by an exponential decay), they

encounter elastic collisions, especially at low r values in the case of a cometary atmosphere with a large production rate, such as in the comet C/1996 B2 (Hyakutake), for example. It follows that the energy distribution function of the excited oxygen atoms presents a thermalized component, resembling the Maxwellian distribution at the ambient gas temperature, plus a nonthermal wing at high energy, also called a hot, superthermal or suprathermal population, in excess of what would be expected from a fully thermal distribution. The relative importance of the thermal core of the distribution and the suprathermal wing depends on the energy released during the production reactions, on the collision frequency and the lifetime of the excited state. In particular, a longer radiative lifetime allows for a stronger degree of thermalization than a short one. It is therefore expected that in the collisional regime of the coma, O(^{1}D) atoms are more efficiently thermalized than O(^{1}S) atoms, whereas, at large r values, none of them would be. It also follows that the Doppler profile of the green and red lines must be broader than the classical Gaussian profile at ambient temperature. This broadening will thus combine with that associated with the expansion motion of the coma, which is usually considered the main spectral broadening process (Cochran 2008).

The existence of a nonthermal population of metastable oxygen has already been brought out by Hubert et al. (2001) and Shematovich et al. (1999) in the Earth thermosphere. These authors showed that the thermospheric O(^{1}D) population has a suprathermal component, and that the degree of thermalization of metastable oxygen depends on altitude through the elastic collision frequency. The existence of suprathermal atoms in a rarefied atmosphere is indeed a general feature that appears when exothermal photochemical reactions are at work, as it was previously shown in the Earth thermosphere for ground state oxygen and nitrogen atoms (Gérard et al. 1991, 1995; Shematovich et al. 1994; Hubert et al. 1996, 1999a).

Formally, the DSMC procedure is a stochastic numerical analog to the Boltzmann integro-differential equation with sources and sinks:

$$\frac{\partial f_{O^*}}{\partial t} + v n\, \nabla_r f_{O^*} + \gamma n\, \nabla_v f_{O^*} = Q_O(r, v, t) + \sum_i J_{\rm el}(f_{O^*}, f_i) + \sum_i J_q(f_{O^*}, f_{\rm i}) - A_{\rm O^*} f_{\rm O^*}, \quad (2)$$

where O* stands for O(^{1}D) or O(^{1}S), index i runs on H_2O, CO_2, CO, and OH, γ is the acceleration due to an external force field, f_{O^*} is the velocity distribution function of species O* (normalized to the local density) and depends on location **r**, velocity **v,** and time t. Q_{O^*} represents the photochemical production rates of O* atoms (including the radiative population of the ^{1}D state by transition from the ^{1}S level), $J_{\rm el}$ represents the elastic collision term, J_q is the quenching rate. Finally, $A_{O^*} f_{O^*}$ is the radiative loss rate, with the Einstein transition parameters $A_{O(^1D)} = A_{630} + A_{636.4} = 0.00563 + 0.00182\ \mathrm{s}^{-1}$ and $A_{O(^1S)} = A_{557.7} = 1.26\ \mathrm{s}^{-1}$ (Wiese et al. 1996). Elastic collisions are treated under the hard sphere approximation, with cross sections listed in Table 2 along with the quenching cross sections (Tenishev et al. 2008). We assumed that the elastic collision cross sections are 10 times larger than the quenching cross sections. The CO_2 cross sections being totally unknown, we used the same cross sections as for H_2O.

The lower boundary of the model is at 10 km of the nucleus center, the gas temperature is assumed to be 50 K, a typical value in cometary atmospheres (Combi et al. 2004), and the model extends up to 5000 km. The density profiles of the major constituents of the coma, namely H_2O, CO, OH, and CO_2 are represented by a Haser model (Equation (3)),

Table 2
Elastic (el) and Quenching (q) Cross Sections (10^{-15} cm^2) for Collisions Between Metastable Atoms and Dominant Species of the Coma (Tenishev et al. 2008)

	H_2O	CO	OH	CO_2
el	1.8	1.5	1.5	1.8
Q	0.18	0.15	0.15	0.18

Note. The same values are assumed for both O(^{1}D) and O(^{1}S), the elastic collision cross section is assumed to be 10 times larger than that for quenching.

$$n_i = \frac{Q_i}{4\pi v_i r^2} e^{-\frac{r}{\beta_i}} \quad i = \mathrm{H_2O, CO, CO_2}$$
$$n_{\rm OH} = \frac{Q_{\rm H_2O}}{4\pi v_{\rm OH} r^2} \frac{\beta_{\rm H_2O}}{\beta_{\rm OH} - \beta_{\rm H_2O}} \left(e^{\frac{-r}{\beta_{\rm H_2O}}} - e^{\frac{-r}{\beta_{\rm OH}}} \right), \quad (3)$$

where n_i, Q_i, v_i, and β_i are, respectively, the number density, the production rate, the expansion velocity, and the destruction scale length of species i. The grid of the model has 100 cells with a quadratic law spacing, so that more cells are used near the nucleus. The model then computes the O(^{1}D) and O(^{1}S) density applying the DSMC method.

The DSMC method described by Bird (1994) consists of a direct simulation of the motion of a restricted set of particles representative of the full gas. Production mechanisms introduce new particles in the model, while loss mechanisms remove them from the simulation. The transportation of particles throughout the modeled gas is also accounted for by exchanges between model cells. Collisions are sampled according to the collision frequency of each process, using a classical acceptance–rejection method. Computation time is limited as much as possible using a common variance reduction technique such that a modeled particle represents several "actual" particles as described by Bird (1994), preserving the statistical properties of the gas. Assuming a steady state, the properties of the modeled system, including the energy distribution function of the suprathermal particles, are estimated statistically using an ensemble average. A detailed description of the modeling method can also be found in Marov et al. (1996).

3. MODEL RESULTS

We simulate the cometary atmosphere of comet C/1996 B2 (Hyakutake) at a 1 AU heliocentric distance under minimum solar activity conditions as a first test case. We use the same parameters as Bhardwaj & Raghuram (2012) for the Haser model of the coma (Table 3). The bulk velocity of OH is smaller than the velocity of OH molecules produced by the phodissociation of H_2O absorbing Lyα photons, which is 1.8 km s^{-1} (Combi 1996). Such a choice is, however, still acceptable since these OH molecules are produced isotropically in the expanding gas and that collisions will slow them down. Indeed, DSMC simulations of Combi (1996) for the conditions of the Giotto flyby of cometP/Halley even show an OH bulk velocity smaller than that of H_2O near the lower boundary of their model, at a 1000 km cometocentric distance.

We perform a one-dimensional (1D) simulation of the photochemistry of the expanding coma with a solar zenith angle

Table 3
Parameters of the Haser Model Used to Represent the C/1996 B2 (Hyakutake) Comet Atmosphere, After Bhardwaj & Raghuram (2012), Biver et al. (1999), and Huebner et al. (1992)

Q_{H_2O}	2.2×10^{29} s^{-1}	β_{H_2O}	8.2×10^4 km
q_{CO}	22%	β_{CO}	1.4×10^6 km
q_{CO_2}	1%	β_{CO_2}	5×10^5 km
v_{bulk}	0.8 km s^{-1}		
$v_{bulk,OH}$	1 km s^{-1}	β_{OH}	1.32×10^5 km

Notes. The CO and CO_2 production rates q_{CO} and q_{CO_2} are given as fractions of the H_2O production rate Q_{H_2O}. The expansion bulk velocity of OH differs from that of H_2O and each species has its own scale length β.

of 0°. Figure 1 shows the computed O(^{1}D) and O(^{1}S) density profiles. The peak O(^{1}S) density is 114 cm^{-3} found at 38 km, while O(^{1}D) has a broad peak around 286 km with a maximum value of 3928 cm^{-3}. Bhardwaj & Raghuram (2012) found a peak O(^{1}S) density of ∼60 cm^{-3} at $r \sim 60$ km and a peak O(^{1}D) density of ∼4000 cm^{-3} near $r = 240$ km. Our Monte Carlo model computes the energy distribution function (EDF) of both species (Figure 2). The Monte Carlo model computes the suprathermal component of the EDF with an energy resolution of 0.01 eV, but a higher resolution is used in this plot to correctly represent the thermal core of the distribution. The nonthermal aspect of the metastable oxygen EDFs is conspicuous at all cometocentric distances. At low r values, the O(^{1}D) EDFs present a thermal core that mimics the Maxwellian EDF at low energy, below ∼0.02 eV. However, as r increases, the importance of the high energy suprathermal component also increases. The O(^{1}S) EDF is also strongly nonthermal at all cometocentric distances. Its degree of thermalization is somewhat less than that of O(^{1}D). Nevertheless, O(^{1}S) has a temperature lower than O(^{1}D) because it is produced with a kinetic energy lower than O(^{1}D): at $r = 286$ km, i.e., near the O(^{1}D) peak, O(^{1}S) has a temperature $T_{O(^1S)} = 360$ K while $T_{O(^1D)} = 469$ K. We note that the metastable oxygen temperature is far above that of the dominant species (i.e., 50 K in our model), highlighting the suprathermal nature of their distribution. We also note quenching can increase the suprathermal nature of the EDFs if the collision frequency is such that particles are quenched before they had a chance to get thermalized. Indeed, the calculated thermalized O(^{1}D) core is somewhat lower at 38 km than at 286 km, a surprising feature that we attribute to quenching. Figure 3 shows the temperature profile of the O(^{1}D) and O(^{1}S) species, isolating that of the hot component. Although the complexity of the detailed EDFs can hardly be summarized with a single number (i.e., the temperature), it appears that both O(^{1}D) and O(^{1}S) are mostly suprathermal at all altitudes, and O(^{1}D) is partly thermalized near the nucleus. The longer radiative lifetime of the ^{1}D state leaves more time to the O(^{1}D) atoms to collide with the thermal dominant molecules, but, on the other hand, O(^{1}S) atoms are produced with a lower kinetic energy. The EDF is then the complex, nonlinear result of the combination of the depth-dependent sources of metastable atoms, the collisional interactions of these atoms with the ambient gas and the radiative decay. O(^{1}S) finally has a computed temperature lower than O(^{1}D).

4. COMPARISON WITH OBSERVATIONS

We will compare the simulation of the coma with two properties known fromobservation: the ratio between the green and red intensities and the spectral width of both emissions.

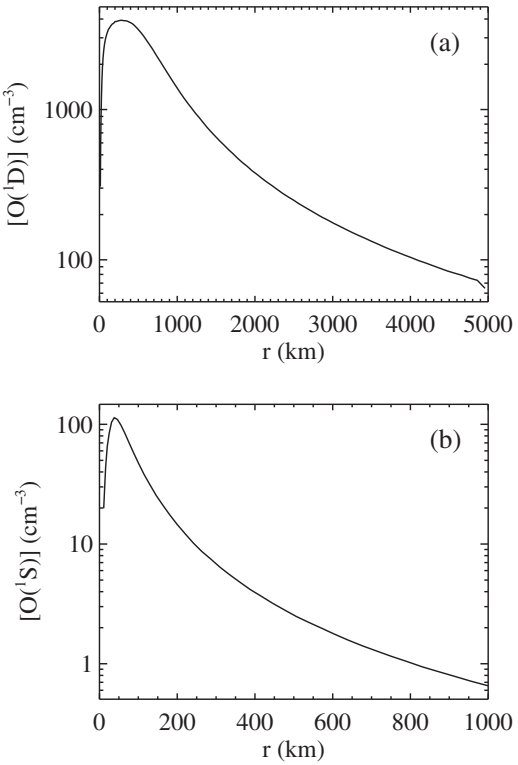

Figure 1. Calculated metastable oxygen (a) O(^{1}D) and (b) O(^{1}S)) density profile for the conditions of comet C/1996 B2(Hyakutake) at 1 AU under minimum solar activity conditions.

The Doppler line profile of a nonthermal population can be calculated based on the energy distribution function, under an assumption of local isotropy:

$$f_d(x) = \int_a^\infty dE \frac{1}{2} \frac{c}{\lambda_0} \sqrt{\frac{m}{2E}} f_E(E) \quad x = \lambda - \lambda_0$$
$$a = \frac{mc^2}{2\lambda_0^2} \left(x \pm \frac{\lambda_0 v_0}{c} \sqrt{1 - \frac{r_0}{r}} \right)^2, \tag{4}$$

where f_E is the energy distribution function of the emitting species, λ_0 is the rest wavelength, f_d is the Doppler line profile of the emission, E the energy, v_0 is the expansion velocity, r_0 is the tangent radius of the considered line of sight, m is the mass of the emitting atom, and c is the speed of light. The + and − signs in the lower bound of integration (a) refer to the two parts of the line of sight where the expansion motion produces either a red or a blue shift due to the projection of the radial bulk velocity vector along the line of sight. Details of the derivation of that result are given in the Appendix. Expression (4) obviously gives the usual Gaussian Doppler profile when f_E is Maxwellian and v_0 is zero. Once the Doppler profile is known at every cometocentric distance used in the model, line-of-sight integration of the emission rate distributed on the appropriate Doppler profile can be performed assuming a spherical symmetry of the coma.

We performed such line-of-sight integration of the 630 and 557.7 nm emissions with a tangent radius of the line of sight chosen at each bin of our model grid. Then the line shape of the emission recorded by an instrument observing the full simulated coma is obtained by summing up the contributions of every line-of-sight geometry accounting for its geometric weight (i.e., proportional to $2\pi r \delta r$ with δr the bin size). The computed line shapes are shown in Figure 4, which also shows the line

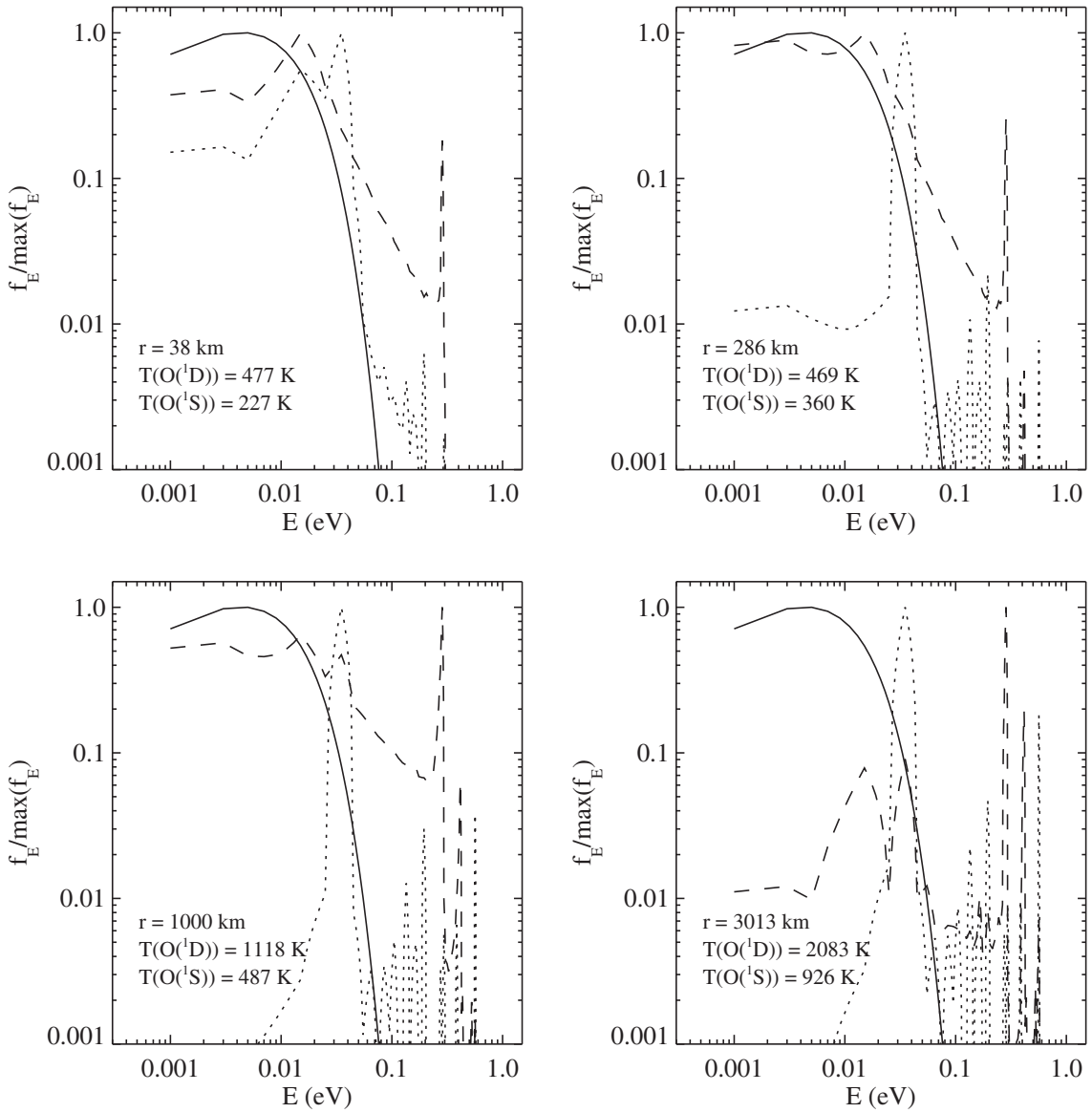

Figure 2. Calculated energy distribution functions (EDFs) of O(^{1}D) and O(^{1}S) at four different cometocentric distances: 38, 241, 1000, and 3013 km. Solid lines represent the Maxwellian EDF at 50 K, i.e., the temperature assumed for the H_2O background gas. The dotted and dashed lines represent the EDFs for O(^{1}S) and O(^{1}D), respectively.

shapes that would be obtained if the coma were not expanding (i.e., assuming a zero expansion velocity). The suprathermal contribution appears as line wings in excess at large Doppler shift, compared with the line shape obtained at the temperature of the ambient gas (i.e., 50 K in our model). The line shapes of the full simulated coma thus appear completely nonthermal. Assuming that a thermal emission does not produce a Gaussian line shape after line-of-sight integration, due to the complicated interplay between the density profile and the projection of the expansion velocity along the observing line of sight, which changes versus *r*. Neglecting the expansion and assuming a thermal emission of course produces Gaussian line shapes.

A comparison between the line shapes computed with and without expansion shows that the radial bulk motion of the coma produces the main contribution to the Doppler broadening of a *thermal* emission, as already pointed out by Cochran (2008). However, in the case of O(^{1}D) and O(^{1}S), the *suprathermal* distribution of the emitted photons produces a Doppler broadening larger than that caused by the expansion. An effective FWHM can be defined for a suprathermal line shape such as those shown in Figure 4 by simply computing the standard deviation of the spectral distribution and computing the FWHM as if the line were Gaussian, which we note FWHM_σ (Table 4). Strictly speaking, this number is not exactly the width of the computed line, but it accounts for the dispersion of the whole line profile. We can then roughly estimate the broadening due to the expansion motion proceeding as if the computed line shape did result from the convolution of two Gaussian functions: the first for the random motion of the particles and the second for the expansion of the coma. If we note FWHM_σ, the width of the computed line that combines both effects (thermal motion and expansion), FWHM^*, the width that we compute when neglecting the expansion of the coma, and $\mathrm{FWHM}_{\mathrm{exp}}$, the width associated with the expansion motion, we can write, as a first approximation:

$$\mathrm{FWHM}_{\mathrm{exp}} \approx \sqrt{\mathrm{FWHM}_\sigma^2 - \mathrm{FWHM}^{*^2}}. \quad (5)$$

In the case of the 6300 Å red line, we compute $\mathrm{FWHM}^* = 0.0488$ Å giving $\mathrm{FWHM}_{\mathrm{exp}} \approx 0.0226$ Å, so that the computed

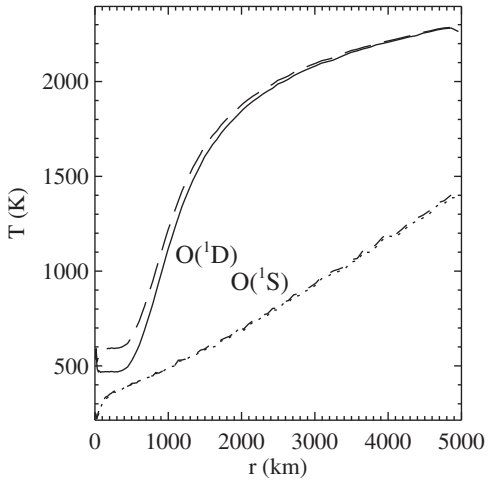

Figure 3. Temperature profile of O(^{1}D) and O(^{1}S) representing the average energy of the modeled EDFs. Solid line: O(^{1}D) temperature. Long dashes: O(^{1}D) temperature, excluding the thermalized core. Dashes: O(^{1}S) temperature. Dotted lines: O(^{1}S) temperature, excluding the thermalized core. The O(^{1}S) dashed and dotted lines closely overlap.

nonthermal line width including the expansion motion is largely dominated by the random motion of the suprathermal particles.

We simulated how the UVES instrument would respond to our computed line shapes shown in Figure 4 and estimated the FWHM that would be fitted on such observations assuming a Gaussian line shape, called $\mathrm{FWHM_{UVES}}$ in Table 4 (i.e., the width of a Gaussian function fitted on the convolution product $f_\mathrm{d}{}^{*}g_\mathrm{uves}$ with f_d the suprathermal line profile and g_uves the UVES instrumental profile). The instrument is assumed to have a Gaussian profile with an FWHM of 0.063 and 0.077 Å at 5577 and 6300 Å, respectively. The standard Gaussian fitting method applied to the simulated data that an instrument such as UVES would produce, induces a small bias in the estimated line width. This is due to the fundamentally non-Gaussian nature of the line shape emitted by the coma. The FWHMs can be used to compute a velocity that, in the case of a Gaussian line profile, corresponds to the most probable velocity of the emitting particles. It is given by (Decock et al. 2013)

$$v_{MP} = \frac{\mathrm{FWHM_{intrinsic}}\,(\lambda)\;c}{\lambda_0 2\sqrt{\ln(2)}}, \qquad (6)$$

where $\mathrm{FWHM_{intrinsic}}(\lambda)$ is the full width at half maximum of the observed spectral line corrected for the instrumental profile. By a misnomer, this number is often called the speed width and noted FWHM(v) (the same formula can also be applied for FWHM_σ). Formally, this velocity is not a width, as it instead corresponds to the most probable speed of a Maxwellian distribution that would produce a Gaussian Doppler line profile having a full width at half maximum equal to $\mathrm{FWHM_{intrinsic}}(\lambda)$. In the case of a cometary atmosphere, the intrinsic width does, however, result from the combination of the expansion motion of the coma (assumed isotropic here) and the spectral line shape of the emitting gas itself, so that the width partly results from the statistically distributed thermal (and suprathermal) motion and partly from the deterministic, hydrodynamic flow expansion.

We point out that the calculated FWHMs, expressed as velocities, predict that the red line should be slightly broader than the green line, in contrast with the observations (Cochran 2008; Decock et al. 2013 and references therein) and in agreement with a previous theoretical analysis (Festou & Feldman 1981). The computed velocity width is 1.58 km s^{-1} for the red line, larger than the value of ∼1 km s^{-1} measured by Cochran (2008). In contrast, the computed width of the green line is 1.02 km s^{-1}, less than the half of the measured value of 2.4 km s^{-1}. Simulating the observation of Cochran (2008) with the appropriate response, we obtain intrinsic speed widths of ∼1.77 and 1.48 km s^{-1} for the red and green lines, which does not account for the observation. The detailed EDFs (Figure 2) and the temperature profile (Figure 3) nevertheless highlight the role that the suprathermal photochemistry, including quenching and thermalization by elastic collisions, plays in the analysis of cometary emissions. It must also be expected that thermalization would be less efficient in the case of a less productive comet. The detailed composition of the coma nevertheless remains an essential factor as well, that controls the mechanisms producing the oxygen atoms as shown by Bhardwaj & Raghuram (2012) and Festou & Feldman (1981), among others. From a quantitative standpoint, we calculate a green/red ratio G/R = 0.078, somewhat smaller than the value adjusted by Bhardwaj & Raghuram (2012), but along the line of observation of other comets (Decock et al. 2013), compatible with G/R = 0.09 measured by Cochran (2008) and smaller than the 0.12–0.16 range of Morrisson et al. (1997). It must, however, be noted that both models use different input solar fluxes and radically different methods, so that the results are not expected to be in perfect agreement. We also note that in the cometocentric range of the MC model, we do not expect that the sources of metastable oxygen neglected here would play a crucial role. At larger distances, however, the dissociative recombination of H_2O^+ can become an important mechanism, capable of producing metastable atoms with a large kinetic energy, thus further broadening the line shapes.

We also simulated the cometary atmosphere of comet 103P/Hartley2 under the observing conditions reported by Decock et al. (2013) on 2010 November 5, i.e., under minimum solar activity conditions, at a nearly unit heliocentric distance and a geocentric distance of 0.16 AU. We simulated the emissions of both the full coma and of the portion of the coma intercepted by the UVES slit, i.e., a $0\farcs44 \times 12''$ aperture as reported by Decock et al. (2013). The water production rate was assumed to be 1.15×10^{28} s^{-1} (Knight & Schleicher 2012) with CO and CO_2 relative abundances amounting to 0.5% and 20%, respectively. Our results are shown in Tables 5 and 6. Simulating the UVES slit or the full coma does not make a significant difference in this case. The computed O(^{1}D) velocity width compares fairly well with the observed value of 1.35 km s^{-1} reported by Decock et al. (2013). However, the simulated O(^{1}S) emission has again a velocity width smaller than that of O(^{1}D) and well below

Table 4
Width of the Computed Green and Red Oxygen Lines for Comet C/1996 B2 (Hyakutake).

Hyakutake Coma	O I–5577 Å		O I–6300 Å	
	Å	km s^{-1}	Å	km s^{-1}
FWHM_σ	0.035	1.14	0.054	1.54
$\mathrm{FWHM_{UVES}}$	0.070		0.095	
$\mathrm{FWHM_{intrinsic}}$	0.032	1.02	0.055	1.58

Notes. FWHMs is the full width at half maximum of a Gaussian function that would have the same standard deviation as the suprathermal line shapes shown in the top panels of Figure 4. FWHMUVES is the width of a Gaussian function fitted on the simulated UVES observation using the suprathermal line shapes of the full simulated coma. FWHMintrinsic is the line width corrected for the UVES response applied to our simulation, as defined by Decock et al. (2013).

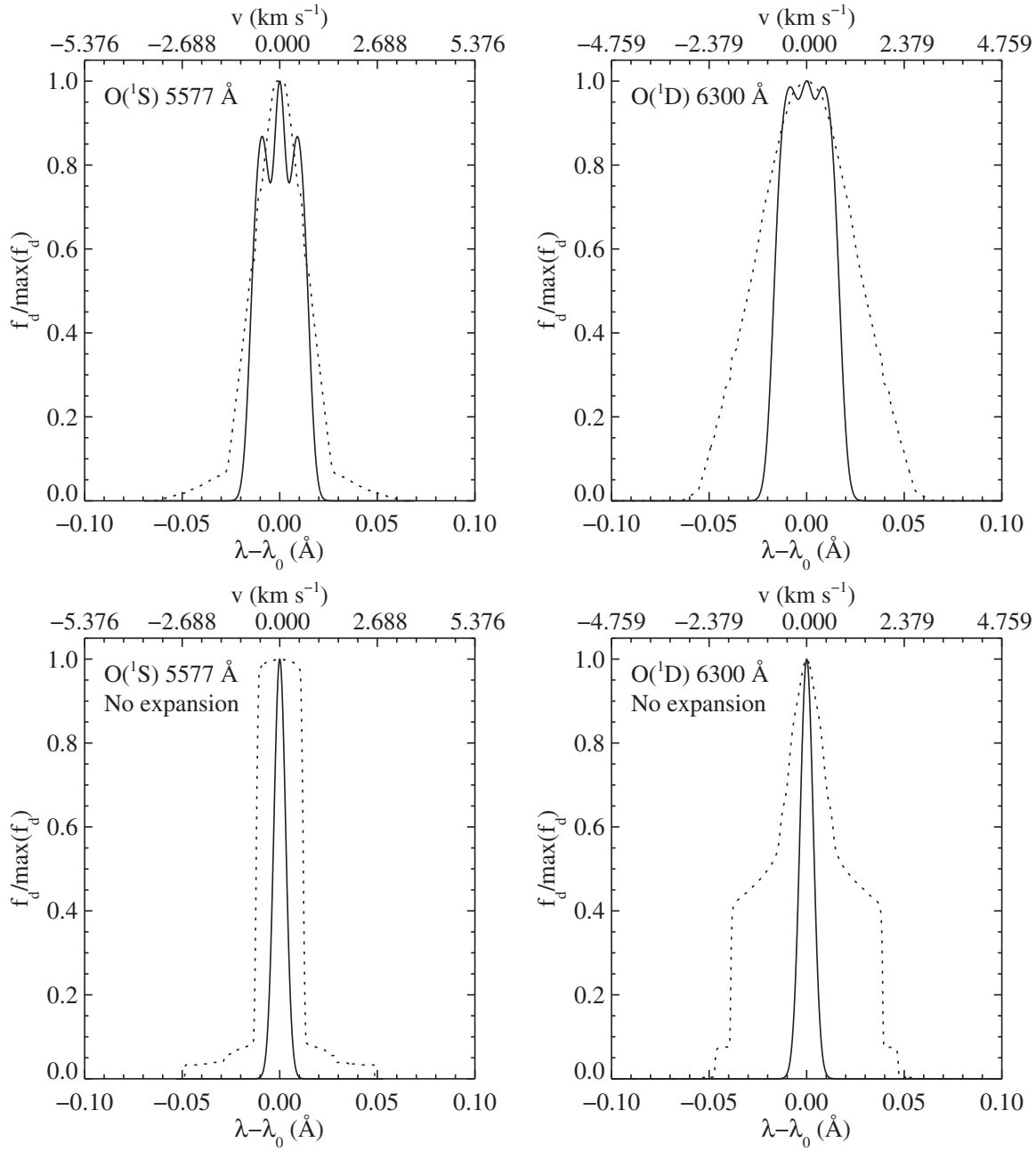

Figure 4. Normalized Doppler line shapes (f_d) of the OI 557.7 and 630 nm emissions integrated over the full coma. Solid lines are obtained assuming thermal emissions at 50 K. Dotted lines represent the line profiles calculated using the metastable oxygen suprathermal energy distribution functions. Both top panels account for the coma expansion while both bottom panels neglect broadening due to the bulk motion. The upper scale gives $v = c\,(\lambda - \lambda_0)/\lambda_0$, i.e., the velocity producing a Doppler shift equal to $\lambda - \lambda_0$ (at first order).

the 2.30 km s^{-1} deduced from the observation. As anticipated above, a less productive comet such as 103P/Hartley2 has a more tenuous atmosphere such that elastic collisions are less frequent and thermalization of the metastable atoms is less efficient, especially concerning O(^{1}D). We also compute a G/R ratio of 0.112 in good agreement with the observed value of 0.09 (Decock et al. 2013).

5. DISCUSSION

We have developed a Monte Carlo model that computes the energy distribution function of metastable oxygen O(^{1}D) and O(^{1}S) in cometary atmospheres. We find that the suprathermal O(^{1}S) and O(^{1}D) populations emit radiation with radically non-Gaussian emission profiles, that combine with the expansion motion of the coma to produce the broad line shape of the full coma at 557.7 and 630 nm. Simulating a very productive comet such as C/1996 B2(Hyakutake) as well as a less productive comet such as 103P/Hartley2, the red line is found to be broader than the green line. We stress that the cross sections needed to calculate the detailed EDFs are sometimes poorly known. In particular, the hard sphere assumption used for elastic collisions certainly departs from the real collision mechanisms which are energy dependent and obey quantum mechanics. In addition, we assume elastic collisions, though a part of the kinetic energy of the colliding fragment may be distributed among the internal degrees of freedom of the colliding partner

Table 5
Same as Table 4 for the Simulation of Comet 103P/Hartley2 for the Full Coma

Hartley 2 Coma	O I–5577 Å		O I–6300 Å	
	(Å)	(km s^{-1})	(Å)	(km s^{-1})
$FWHM_{\sigma}$	0.0448	1.445	0.0559	1.598
$FWHM_{UVES}$	0.0752		0.0962	
$FWHM_{intrinsic}$	0.0412	1.329	0.0576	1.645

Table 6
Same as Table 4 for the Simulation of the UVES Slit Projected on the Coma of Comet 103P/Harley 2

Hartley 2 UVES Slit	O I–5577 Å		O I–6300 Å	
	(Å)	(km $s^{-1)}$	(Å)	(km s^{-1})
$FWHM_{\sigma}$	0.0439	1.416	0.0553	1.581
$FWHM_{UVES}$	0.0748		0.0962	
$FWHM_{intrinsic}$	0.0403	1.302	0.0577	1.650

Notes. All numbers are given with an accuracy that allows a comparison between Tables 5 and 6, although it is not expected that our computed results are accurate enough to reach such a significance level.

of the metastable oxygen atoms. In particular, H_2O, CO_2, CO, and OH can be excited in rotation and vibration. The excitation of molecular rovibrationnal levels during the collisions would consume a part of the kinetic energy of the interacting partners and could thus enhance the thermalization rate of the colliding suprathermal metastable oxygen atoms, particularly considering O(^{1}D), which has a longer radiative lifetime. The detailed quantitative results regarding the line's FWHMs may thus be subject to corrections when the needed cross sections are known. Also, uncertainties on the solar flux are important sources of uncertainties in any photochemical model.

The width of the red line obtained using the model is too broad, while that of the green line is too narrow. We compute a velocity width of 1.58 km s^{-1} for the O(^{1}D) 630 nm line of comet 103P/Hartley 2, larger than the observed values ranging between 1.23 and 1.35 km s^{-1} (Decock et al. 2013). This suggests that the value used for the elastic collision cross section is too low so that the model underestimates the O(^{1}D) thermalization rate. An overestimate of the O(^{1}D) photoproduction rate at short wavelengths can also result in an overestimate of the line width. The velocity width that we compute for the green emission of comet 103P/Hartley2 is $\sim$1.4 km s^{-1}, much narrower than the values of $\sim$2.3 km s^{-1} reported by Decock et al. (2013), who also report observations of other comets for which the oxygen 557.7 nm line is nearly twice as broad as that of 103P/Hartley2. More energetic O(^{1}S) production mechanisms would contribute to resolve that discrepancy. Decock et al. (2013) suggested that a more important contribution of the solar photons between 80 and 100 nm in the photodissociation process could be a possibility. For example, the energy of a photon of the O II line at 83.4 nm is $\sim$14.9 eV, nearly 50% larger than the 10.2 eV of a Lyα photon. At still shorter wavelengths, the relatively bright solar helium line at 58.4 nm corresponds to photons of $\sim$21.3 eV, which are also capable of producing very fast moving atoms in a photodissociation process. Another possibility would be that the branching ratio of the O(^{1}S) production channel would significantly increase as the wavelength of the absorbed photon decreases, thus favoring the production of faster O(^{1}S) and slower O(^{1}D) atoms. Only quantum mechanics computations could determine the details of the photodissociation mechanism with their dependence versus the wavelength of the absorbed photon. A modification of the composition of the coma can also help broaden the modeled green line by favoring species such as CO_2, CO, and OH, which produce more energetic O(^{1}S) atoms. The collision frequency depends on the cross section, the density, and the temperature (through the relative velocity of the colliding partners). These three parameters can be considered to modify the line's width. However, the cross sections are the most poorly known of the three parameters and are the best candidates to reduce the red width without further reducing the green width.

We conducted preliminary sensitivity tests suggesting that a multiplication of the elastic collision cross sections by $\sim$30 would reduce the computed width to $\sim$1 km s^{-1} for comet C/1996 B2 (Hyakutake), while multiplication by $\sim$100 would reduce the computed velocity width to $\sim$1.3 km s^{-1} in the case of 103P/Hartley 2. We also conducted a simulation test with an artificial increase of the average kinetic energy of the O(^{1}S) atoms to 0.09 eV, which produced an increase of the simulated FWHM to $\sim$1.5 km s^{-1} for both comets C/1996 B2 (Hyakutake) and 103P/Hartley 2, suggesting that including more energetic sources is a promising option.

The spherical symmetry assumption is also an issue: under a solar zenith angle larger than 0°, unit optical thickness will be reached at higher cometocentric distance for photons with given wavelengths absorbed by the coma gas. These photons are thus absorbed at somewhat larger cometocentric distances, where the collision frequency and thermalization rate are lower, thus producing populations of excited species with broader line shapes. This implies a cylindrical symmetry along the comet–Sun axis instead of a spherical symmetry, as it is assumed here.

We also note that the calculated suprathermal emissions of comet C/1996 B2 (Hyakutake), produced if observed using the UVES spectrograph, assumes that the coma would fill the instrument's field of view, which is not realistic and slightly influences the computed intrinsic width. Indeed, our simulation of comet 103P/Hartley 2, accounting for a realistic observing geometry, shows little difference with the full coma integration. Nevertheless, it remains that our model shows one of the deep mechanisms contributing to the width of observed spectral lines that tends to leave a broad green O(^{1}S) line while narrowing the red O(^{1}D) emission: the O(^{1}D) atoms have a radiative lifetime longer than O(^{1}S), and are more efficiently thermalized by elastic collisions, which reduces the width of the red line more strongly than the green one. We also show that the suprathermal Doppler line profile produces a broadening larger than that caused by the expansion of the coma, which is an unexpected result. The chemical composition of the coma is obviously a key element of the modeling, and a source of uncertainties. For example, an increased CO_2 abundance favors the production of faster O atoms (compared with H_2O) because the produced oxygen atoms take up a larger fraction of the available kinetic energy owing to the large mass of the second fragment (CO). It can be expected that the future *Rosetta* mission of ESA, now heading toward comet 67P/Churiumov–Gerasimenko (Davidsson & Gutiérrez 2005), will soon provide detailed and reliable measurements of the composition, using the on board mass spectrometer. These future observations used in parallel with the data from ground based measurements, will provide an unprecedented opportunity to extensively test the ability of photochemical models to account for the properties of the observed emissions of the coma.

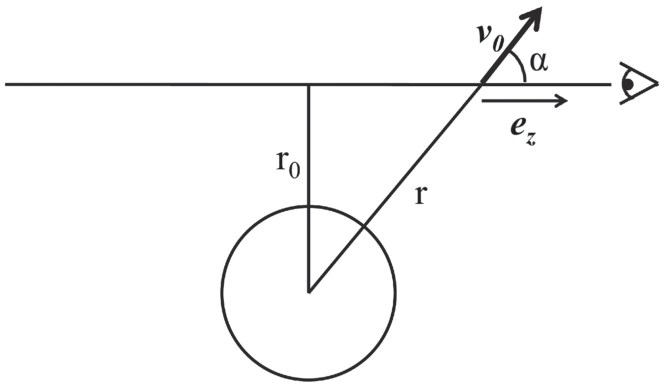

Figure 5. Geometry used to represent the expanding coma for computation of the distribution of the Doppler shift. The observer is represented by an eye on the right side, vector v_0 represents the expansion velocity, unit vector e_z is oriented toward the observer. The tangent point of the line of sight, i.e., the point of closest approach to the comet center, is at a distance r_0 from the comet center, and we study the emission of a small gas volume located on the line of sight at a distance r from the center of the comet.

6. CONCLUSIONS

1. The Monte Carlo computation of the metastable oxygen photochemistry shows that both O(^{1}S) and O(^{1}D) have a suprathermal distribution in the cometary atmosphere. This distribution can be partly thermalized near the nucleus of very productive comets.
2. The degree of thermalization of O(^{1}D) is higher because the productivity is large, especially at low cometocentric distance, whereas O(^{1}S) is nearly not thermalized, owing to its lower radiative lifetime.
3. The width of the 630 nm and 557.7 nm cometary emissions is dominated by the suprathermal distribution of the metastable O(^{1}D) and O(^{1}S) atoms, rather than by the expansion motion.
4. Current knowledge of cometary photochemistry and composition does not explain that the green line at 557.7 nm emitted by the coma is broader than the red line at 630 nm.

D. V. Bisikalo and V. I. Shematovich were partially supported by the Russian Academy of Sciences (Program-22), and by the Russian Foundation for Basic Research (Project 14-02-00838). B. Hubert, D. Hutsemékers, and E. Jehin are supported by the Belgian FRS-FNRS. This work was supported by the FRFC grant no. 2.4541.11. A. Decock acknowledges the support of the Belgian National Science Foundation F.R.I.A., Fonds pour la formation à la Recherchedansl'Industrie et l'Agriculture. The authors thank the reviewer for very helpful comments.

APPENDIX

In this section, we explicitly show how the expression for the Doppler profile of a nonthermal gas is obtained, accounting for the bulk speed (Equation (4)). This calculus relies on the following result demonstrated by Hubert (1999).

Let $X_1, \ldots, X_n$ be random variables having distribution function f_X ($x_1, \ldots, x_n$) and taking values in intervals $\Omega_1, \ldots, \Omega_n$ respectively. Let also Y be a random variable which, for $X_1, \ldots, X_n$ having determined values, can be computed as $Y = \Phi(X_1, \ldots, X_n)$. The distribution function followed by variable Y is given by

$$f_Y(y) = \int_{\Omega_1} dx_1 \ldots \int_{\Omega_n} dx_n f_X(x_1, \ldots, x_n) \times \delta(y - \Phi(x_1, \ldots, x_n)), \quad \text{(A1)}$$

where δ represents the Dirac distribution. This result is indeed rather natural and it is easily generalized to multiple dimensions for a set of variables $Y_1, \ldots, Y_n$.

We can apply result A1 to the case of the Doppler effect affecting photons emitted by an isotropic gas with an energy distribution function $f_E(E)$ and moving at velocity $\mathbf{v_0}$ with respect to an observer. In particular, we use a geometric representation appropriate to the case of an expanding cometary atmosphere (Figure 5). We consider an observer looking at the coma along a line of sight of tangent cometocentric distance r_0, and we compute the Doppler distribution of the wavelength (λ) of photons at rest wavelength λ_0 emitted by atoms (or molecules) of mass m of a small gas volume located on the line of sight at a distance r from the nucleus. Such a definition requires us to separately treat the left- and right-hand sides of the line of sight about the tangent point. We further assume that the emitting gas moves at a velocity $\mathbf{v_0}$ in the radial direction. We assume that the gas has an isotropic velocity distribution function in a frame of reference moving at velocity $\mathbf{v_0}$, such that its energy distribution function is $f_E(E)$ in that frame of reference, and that collisional broadening is negligible.

The z component of vector v_0 is $v_{0z} = v_0 \cos(\alpha)$, with α as the polar angle of vector v_0 from the z direction. On the right-hand side of the line of sight (Figure 5), $\cos(\alpha) = \sqrt{1 - r_0^2/r^2}$ and the expansion motion produces a blue shift, while on the left-hand side, it is $\cos(\alpha) = -\sqrt{1 - r_0^2/r^2}$ and the expansion motion produces a red shift. We can write

$$v_{0z} = \pm\sqrt{1 - \frac{r_0^2}{r^2}}\, v_0. \quad \text{(A2)}$$

For nonrelativistic velocities, the Doppler-shift of a photon emitted toward the observer is given by

$$x = \lambda - \lambda_0 = -\lambda_0 \frac{V_z}{c}, \quad \text{(A3)}$$

with c as the speed of light, and V_z as the z component of the velocity of the emitting particle given by $V_z = v_z + v_{0z}$, where v_z is the z component of the thermal velocity. If the energy of the emitting particle is E and the polar angle of the velocity from the z direction is θ, we can write the Doppler shift as

$$x = \left(\sqrt{\frac{2E}{m}}\cos(\theta) + v_{0z}\right)\frac{\lambda_0}{c}. \quad \text{(A4)}$$

Applying result (A1) under the assumption of an isotropic velocity distribution function (in the frame of reference moving at velocity v_0), we obtain, using the azimuth and polar angles φ and θ:

$$f_d(x) = \int_0^{2\pi} d\varphi \int_0^{\pi} d\theta \int_0^{\infty} dE \frac{1}{4\pi} \sin(\theta) f_E(E) \times \delta\left(x - \left(-\lambda_0 \frac{\sqrt{\frac{2E}{m}}\cos(\theta) + v_{0z}}{c}\right)\right). \quad \text{(A5)}$$

Integration versus φ is straightforward:

$$f_d(x) = \int_0^{\pi} d\theta \int_0^{\infty} dE \frac{1}{2} \sin(\theta) f_E(E) \times \delta\left(x + \frac{\lambda_0}{c} v_{0z} + \frac{\lambda_0}{c}\sqrt{\frac{2E}{m}}\cos(\theta)\right). \quad \text{(A6)}$$

The general efficient strategy to apply to deal with such an integral is to keep all integration variables, but one constant, and apply a variable change on that last variable, that easily allows the integration on the new variable to be reduced to either one or zero using the properties of the Dirac distribution. For E given, let us define

$$q = \frac{\lambda_0}{c}\sqrt{\frac{2E}{m}}\cos(\theta) \text{ such that } dq = -\frac{\lambda_0}{c}\sqrt{\frac{2E}{m}}\sin(\theta)\, d\theta. \quad \text{(A7)}$$

Integral (A6) becomes

$$f_d(x) = \int_0^{\infty} dE \int_{-\frac{\lambda_0}{c}\sqrt{\frac{2E}{m}}}^{\frac{\lambda_0}{c}\sqrt{\frac{2E}{m}}} dq \frac{1}{2}\frac{c}{\lambda_0}\sqrt{\frac{m}{2E}} f_E(E) \times \delta\left(q - \left(-\frac{\lambda_0}{c} v_{0z} - x\right)\right). \quad \text{(A8)}$$

Integration versus variable q is one when

$$-\frac{\lambda_0}{c}\sqrt{\frac{2E}{m}} < -\frac{\lambda_0}{c} v_{0z} - x < \frac{\lambda_0}{c}\sqrt{\frac{2E}{m}} \quad \text{(A9)}$$

and zero otherwise. Condition (A9) is true when, $E > \left(mc^2\right) / \left(2\lambda_0^2\right)(x + \lambda_0 v_{0z}/c)^2$ so that integral (A8) reduces to

$$f_d(x) = \int_{\frac{mc^2}{2\lambda_0^2}\left(x+\frac{\lambda_0}{c} v_{0z}\right)^2}^{\infty} dE \frac{1}{2}\frac{c}{\lambda_0}\sqrt{\frac{m}{2E}} f_E(E). \quad \text{(A10)}$$

Now, replacing v_{0z} by its value (A2) and accommodating the $\pm$ signs so that the upper sign refers to the right-hand part of the line of sight, we obtain

$$f_d(x) = \int_{\frac{mc^2}{2\lambda_0^2}\left(x \pm \frac{\lambda_0}{c}\sqrt{1-\frac{r_0^2}{r^2}} v_0\right)^2}^{\infty} dE \frac{1}{2}\frac{c}{\lambda_0}\sqrt{\frac{m}{2E}} f_E(E), \quad \text{(A11)}$$

i.e., the result given in Equation (4).

REFERENCES

Bhardwaj, A., & Raghuram, S. 2012, ApJ, 748, 13
Bird, G. A. 1994, in Molecular Gas Dynamics & The Direct Simulation of Gas Flows (Oxford: Clarendon),
Bisikalo, D. V., Marov, M. Ya., Shematovich, V. I., & Strel'nitsij, V. S. 1989, AdSpR, 9, 53
Biver, N., Bockelée-Morvan, D., Crovisier, J., et al. 1999, AJ, 118, 1850
Cochran, A. L. 2008, Icar, 198, 181
Combi, M. R 1996, Icar, 123, 207
Combi, M. R., Harris, W. M., & Smyth, W. H. 2004, in Comets II, ed. M. Festou, H. U. Keller, & H. A. Weave (Tucson, AZ: Univ. Arizona Press), 523r
Davidsson, B. J. R., & Gutiérrez, P. J. 2005, Icar, 176, 453
Decock, A., Jehin, E., Hutsemékers, D., & Manfroid, J. 2013, A&A, 555, id.A34, doi: 10.1051/0004-6361/201220414
Dekker, H., D'Odorico, S., Kaufer, A., Delabre, B., & Kotzlowski, H. 2000, Proc. SPIE, 4008, 534
Ehrenfreund, P., & Charnley, S. B. 2000, ARA&A, 38, 427
Festou, M. 1981, A&A, 96, 52
Festou, M., & Feldman, P. D. 1981, A&A, 103, 154
Gérard, J. C., Shematovich, V. I., & Bisikalo, D. V. 1991, GeoRL, 18, 1695
Gérard, J. C., Shematovich, V. I., & Bisikalo, D. V. 1995, in Geophysical Monograph, Vol 87 (Washington, DC: AGU), 235
Hubert, B. 1999, Etude de signatures radiatives de populations d'atomes superthermiques dans la thermosphère terrestre a thesis (in French)
Hubert, B., Gérard, J. C., Shematovich, V. I., & Bisikalo, D. V. 1996, GeoRL, 23, 2215
Hubert, B., Gérard, J. C., Cotton, D. M., Bisikalo, D. V., & Shematovich, V. I. 1999, JGR, 104, 17139
Hubert, B., Gérard, J. C., Killeen, T. L., et al. 2001, JGR, 106, 12753
Huebner, W.F., Keady, J. J., & Lyon, S. P. 1992, Ap&SS, 195, 1
Knight, M. M., & Schleicher, D. G. 2012, Icar, 222, 691
Marov, M. Ya., Shematovich, V. I., & Bisikalo, D. V. 1996, SSRv, 76, 1
Morrisson, N. D., Knaught, D. C., Mullis, C. L., & Lee, W. 1997, PASP, 109, 676
Raghuram, S., & Bhardwaj, A. 2012, Icar, 223, 91
Rubin, M., Tenishev, V. M., Combi, M. R., et al. 2011, Icar, 213, 655
Shematovich, V. I., Bisikalo, D. V., & Gérard, J. C. 1994, JGR, 99, 23217
Shematovich, V. I., Gérard, J. C., Bisikalo, D. V., & Hubert, B. 1999, JGR, 104, 4287
Swings, P. 1962, Ann. Astrophys., 25, 165
Tenishev, V., Combi, M. R., & Rubin, M. 2001, ApJ, 732, 104
Tenishev, V., Combi, M. R., & Davidsson, B. 2008, ApJ, 685, 659
Wiese, W. L., Fuhr, J. R., & Deters, T. M. 1996, JPCRD, 7, 532